Available online at www.sciencedirect.com

SciVerse ScienceDirect

Scripta Materialia 66 (2012) 250–253

Scripta MATERIALIA

www.elsevier.com/locate/scriptamat

# Modeling of large strain hardening during grain refinement

C.F. Gu,[a,*] L.S. Tóth[b] and B. Beausir[b,c]

[a] *Department of Materials Engineering, Monash University, VIC. 3800, Australia*
[b] *LEM3, CNRS UMR 7239, UPV Metz, Ile du Saulcy, 57045 Metz Cedex 1, France*
[c] *Institut für Strukturphysik, Technische Universität Dresden, D-01062 Dresden, Germany*

Received 30 June 2011; revised 7 September 2011; accepted 3 November 2011
Available online 12 November 2011

Strain hardening was modeled at large strains taking into account the geometrically necessary dislocations (GNDs) with the help of a recent grain refinement model. The GND density was studied experimentally with orientation imagining for oxygen-free high-conductivity copper deformed in equal channel angular pressing and in simple shear to the same equivalent strain. The results show that the GND density can be predicted fairly well by the model in accord with experiments, and also affects stage IV hardening.


*Keywords:* Strain hardening; Geometrically necessary dislocation; OFHC copper; Simple shear; Grain refinement modeling

Experiments and modeling show that strain hardening behavior is microstructure dependent and the most relevant parameter is the heterogeneous dislocation density which develops a cell structure by self-organization of the dislocations [1]. The first widely used model is the Kocks model, which assumes only a homogeneous (average) dislocation density together with the mean free path of dislocation motion [2]. For large strain hardening, Estrin et al. [3] and Tóth et al. [4] considered the composite nature of the dislocation cell structure and showed that the sharpening of the dislocation walls (i.e. the experimentally observed decrease in their volume fraction) can account for stage IV hardening. Rollett and coworkers [5] could explain stage IV by incorporating the role the dislocation debris in strain hardening. Pantleon has shown that by incorporating the geometrically necessary dislocations (GNDs) in the Kocks approach, stage IV can also be obtained [6,7]. At large strains, where grain refinement is in progress, the GNDs are of great importance as they provide a continuous increase of subgrain boundary misorientations. It is therefore important to study the effect of GNDs on hardening simultaneously with grain refinement.

Recently a quantitative polycrystal grain refinement (GR) model was proposed which is capable of predicting texture, grain size, strain hardening and next-neighbor disorientations from the refined grains in a single modeling frame [8]. The model is based on the lattice curvature that develops mostly near the grain boundaries as the result of a slow-down of the strain-induced lattice rotation of an embedded crystal. Several applications of the model proved its pertinence [9–12].

In the present work, we aim to investigate the hardening behavior predicted by the GR model. During simulation, the only parameter that controls the rate of the grain refinement process – called $\mu$ – is the retardation of the lattice rotation at the grain boundary. Its value can be in the range between 0.5 and 1; $\mu = 1$ was used here. The GR model predicts the geometrically necessary dislocations that have to be present in the crystal to develop the curvature of the lattice. The necessary populations of GNDs for the described mechanism of the lattice curvature were named curvature-induced dislocations (CIDs) in Ref. [8]. Another population of GNDs are those redundant dislocations that build disorientation across dislocation cell walls. Their origin is stochastic, made by the bias of the dislocation fluxes coming to the wall from two opposite directions [6,13]. Pantleon showed that such GNDs affect stage III only slightly and do not affect stage IV at all [7]. The density of both kinds of GNDs can be obtained quantitatively from the GR model. The CID-made lattice curvature can be extracted from electron backscatter diffraction (EBSD) orientation maps and can be compared to the prediction.

Oxygen-free high-conductivity copper was heat-treated at 650 °C for 2 h, resulting in an average grain size of about 24 μm. The billet of the annealed copper was

* Corresponding author. Fax: +61 03 990 54940; e-mail: Chengfan.Gu@monash.edu

1359-6462/$ - see front matter © 2011 Acta Materialia Inc. Published by Elsevier Ltd. All rights reserved.
doi:10.1016/j.scriptamat.2011.11.002

processed by one-pass equal channel angular pressing (ECAP). The EBSD measurements were performed using a JEOL 7001F with an HKL detector with a step size of 0.1 μm. Boundaries were identified using a minimum disorientation angle of 5° between adjacent pixels. In order to obtain a strain hardening curve in the intersection plane of the channels in the ECAP die, torsion tests were carried out on cylindrical samples of 6 mm diameter and 15 mm length to simulate the simple shear deformation mode of ECAP by torsion. To obtain the stress–strain curve from the measured twisting angle and the torque in torsion, the Nadai formula [14] was used.

The GND scalar density can be defined as the entry-wise norm of the Nye dislocation density tensor ($\alpha$) [15] divided by the Burgers vector length:

$$\rho_{\mathrm{GND}} = \frac{1}{b}\sqrt{\alpha_{ij}\alpha_{ij}} \tag{1}$$

Five components of the Nye tensor can be determined from two-dimensional mapping. From them, a truncated scalar value of $\rho_{\mathrm{GND}}$ can be calculated, which we call $\rho_{\mathrm{GND}}^{(2D)}$:

$$\rho_{\mathrm{GND}}^{(2D)} = \frac{1}{b}\sqrt{\alpha_{12}^2 + \alpha_{13}^2 + \alpha_{21}^2 + \alpha_{23}^2 + \alpha_{33}^2} \tag{2}$$

In order to estimate $\rho_{\mathrm{GND}}$ for the three-dimensional case, we assume $\alpha$ to be isotropic and obtain $\rho_{\mathrm{GND}} = 3\rho_{\mathrm{GND}}^{(2D)}/\sqrt{5}$ by division of Eqs. (1) and (2). The EBSD map was analyzed using the method proposed by Pantleon [16] to obtain the measurable $\alpha_{ij}$ components. For quantification of GNDs only within the grain interiors, the adjacent pixels across boundaries displaying a disorientation exceeding 5° were not considered. The obtained GND densities using a color code with the help of the EBSDmcf Software [17] are displayed in Figure 1. For densities smaller than 10% of the maximum, the color code was not used; instead, the band contrast was plotted ("BC" in Fig. 1; the total surface where the density is less than 10% of its maximum value represents 49.5% of the total area). It is apparent that the GND density shows a patterning structure in which most of the GNDs are grouping into "walls" where their local density is very high. The approximate average distance between these walls is about 2 μm. These walls are most probably the precursors of new grain boundaries. They are more frequent near the grain boundaries of the original grains (see Fig. 1). The maximum GND density value is $3.35 \times 10^{15}\ \mathrm{m}^{-2}$ in the map and the average value of $\rho_{\mathrm{GND}}$ on the map is $4.38 \times 10^{14}\ \mathrm{m}^{-2}$; the entire measured surface was considered in the calculation of the average.

For the simulation of hardening, the GR model was employed in which hardening was simulated with the dislocation cell-based composite model [3,4]. Several populations of dislocations were considered in the model: dislocation density in the cell interior ($\rho_c$) and in the cell wall ($\rho_w$), and the CID density ($\rho_{\mathrm{CID}}$). The wall density can be split into two populations ($\rho_w = \rho_{ws} + \rho_{wg}$), where $\rho_{ws}$ is the statistical wall dislocation density and $\rho_{wg}$ is the GNDs that build up misorientation across the cell wall. Transmission electron microscopy measurements show that these cell misorientations are relatively small [18]. Nevertheless, their contribution is present in the dislocation density tensor, which can be measured by the EBSD technique described above. We used the same evolution equations as in Ref. [8] for $\rho_c$, $\rho_{ws}$ and $\rho_{wg}$.

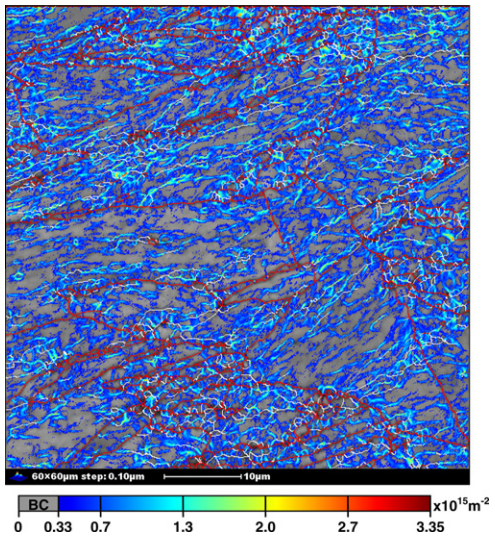


**Figure 1.** Map of GND density obtained from EBSD measurement after one-pass ECAP on the ND plane. Boundaries with at least 15° disorientation are marked with red lines while those that are between 5 and 15° are colored white. For intensities less than $0.33 \times 10^{15}\ \mathrm{m}^{-2}$, the BC was plotted.

The sharpening of the cell walls is expressed by decreasing their volume fraction according to the formula introduced in Ref. [3]: $f = f_\infty + (f_0 - f_\infty)\exp(-\gamma_r/\tilde{\gamma}_r)$, where $f_0$ is the initial value of $f$, and $f_\infty$ is its saturation value at large strains. The quantity $\tilde{\gamma}_r$ describes the rate of decrease of $f$. The same values of parameters as those used in Ref. [3] were employed in the present study ($f_0 = 0.25$, $f_\infty = 0.06$ and $\tilde{\gamma}_r = 3.2$). There are several parameters that control different dislocation mechanisms (for details, see [8,13]: $\alpha^*$, $\beta^*$, $k_0$, $\xi_1$ and $\xi_2$. $\xi_1$ and $\xi_2$ are numerical parameters that describe the fractions of statistical dislocations that contribute to the buildup of cell misorientations. This misorientation can be obtained from the expression $\theta = bd\rho_{wg}$. Finally, the $k_0$ parameter controls the dislocation annihilation rate. The average dislocation density is defined for the dislocation cell structure as follows:

$$\rho_{\mathrm{average}} = \rho_{CID} + f(\rho_{ws} + \rho_{wg}) + (1 - f)\rho_c \tag{3}$$

The dislocation cell size is related to the total dislocation density according to Holt's formula:

$$d = H/\sqrt{\rho} \tag{4}$$

where the $H$ parameter is about 10 for copper [19].

The density of CIDs is estimated in the present version of the GR model using the basic formula:

$$\rho_{\mathrm{CID}} = C\frac{n}{bR}, \tag{5}$$

where $R$ is the lattice curvature induced by the presence of one grain boundary and $n$ is the number of near grain boundaries that can also induce lattice curvatures. $n$ can be as high as 3 for a "corner" region of the grain, taking an initial cubic shape. For the calculation of $R$ and $n$, see the original work on the GR model [8]. $C$ is a parameter in Eq. (5), and can take a value of less than 1. This

**Table 1.** Parameters for the calculation of strain hardening during grain refinement.

| $\rho_{co}$ ($m^{-2}$) | $\rho_{w0}$ ($m^{-2}$) | $\tau_0$ (MPa) | $f_0$ | $\bar{\gamma}$ | $m$ | $n$ | $\dot{\gamma}_0$ ($s^{-1}$) | $\alpha$ | $G$ (GPa) | $b$ (nm) | H | $\xi_1$ | $\xi_2$ | $k_0$ | $\alpha^*$ | $\beta^*$ | C |
|---|---|---|---|---|---|---|---|---|---|---|---|---|---|---|---|---|---|
| $10^{13}$ | $10^{14}$ | 30 | 0.25 | 3.2 | 20 | 10 | 1 | 0.25 | 47.4 | 0.256 | 10 | 0.1 | 0.05 | 2.0 | 0.015 | 0.002 | 0.1 |

parameter expresses the fact that the CIDs are progressively building up new grain boundaries, thus, all of them cannot be present at the same time in the crystal in a homogeneous distribution. This is clearly demonstrated in Figure 1 by the inhomogeneous distribution of the GNDs. The $(1-C)$ portion of the CIDs is integrated into the new grain boundaries (and are producing increasing disorientations), while the portion represented by $C$ can be considered to be distributed nearly homogeneously at any given time. The possible effect on hardening of the CID walls evidenced in Figure 1 is ignored in the present model because their spacing is much larger than the cell size, so it is the cell structure which determines the strength of the material. Indeed, the predicted cell size is 0.405 μm at the end of strain (see below) while the spacing of these walls – where they are more or less regular – is about 2 μm. Note also that these walls do not exceed 5° misorientations.

In the present model, the CID obtained from Eq. (5) contributes to the strength of the cell ($\tau_c$) and wall regions ($\tau_w$) using the rate-sensitive Taylor formula in both the cell and wall regions:

$$\tau_c = \tau_0 + \alpha G b \sqrt{\rho_c + \rho_{\mathrm{CID}}} \left(\frac{\dot{\gamma}_r}{\dot{\gamma}_0}\right)^m,$$
$$\tau_w = \tau_0 + \alpha G b \sqrt{\rho_w + \rho_{\mathrm{CID}}} \left(\frac{\dot{\gamma}_r}{\dot{\gamma}_0}\right)^m \quad (6)$$

Here $m$ is the strain rate sensitivity of slip and $\tau_0$ is the initial resolved shear strength of the crystal. The resultant strength is obtained from the composite model:

$$\tau_{res} = f\tau_w + (1-f)\tau_c \quad (7)$$

The stress necessary for the plastic deformation of a grain is proportionally determined by the $\tau_{\mathrm{res}}$ value of the crystallographic slip obtained from Eq. (7) in the polycrystal plasticity code. Knowing the prescribed plastic strain rate $\dot{\bar{\varepsilon}}$ (totally imposed), the equivalent stress is obtained from the condition of conjugant plastic work:

$$\bar{\sigma} = (\underline{\underline{\sigma}} : \underline{\underline{\dot{\varepsilon}}})/\dot{\bar{\varepsilon}}_{VM} \quad (8)$$

where $\dot{\bar{\varepsilon}}_{VM}$ is the von Mises equivalent strain rate.

During the simulation, that part of a grain which reaches 5° disorientation with respect to its parent grain orientation is considered to be a new grain. This new grain is supposed to be free of CIDs. This hypothesis is supported by Figure 1, which shows that the distribution of CIDs is not homogeneous; the CIDs are grouped into walls at a scale that is about 6 times larger than the dislocation cell walls. Between these CID walls the CID density is very low (see Fig. 1) and can be considered to be homogeneous. When a new grain is "born", it is born from these CID walls, so the CID density inside those new grains can be ignored and the hypotheses of the grain refinement model can be applied. An overall curvature is in fact predicted by the model. However, it is not a uniform curvature but varies locally because of the grouping of the CID dislocations into the walls.

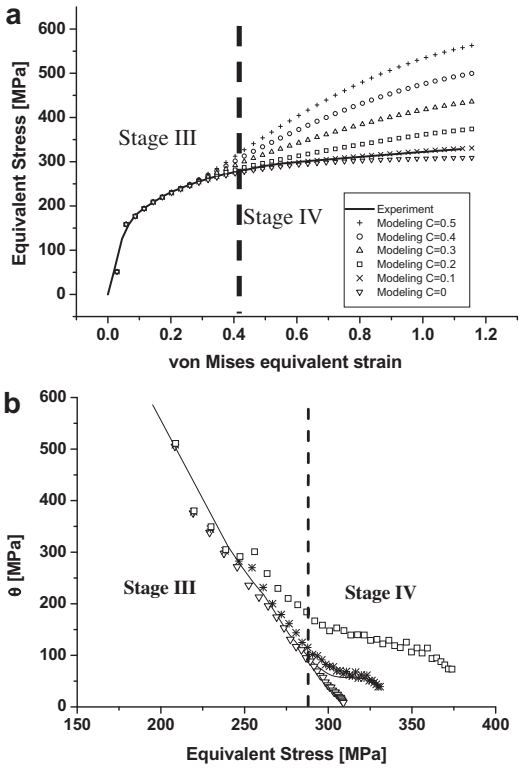


**Figure 2.** Experimental (continuous line) and simulated hardening curves (symbols) for copper for different values of the $C$ parameter. (a) Stress–strain curves; (b) hardening rates for $C = 0.0$, 0.1 and 0.2, together with the experimental rate (continuous line).

For all these reasons, the new grain is initially supposed not have lattice curvature. This procedure is repeated at several levels: four embedded grain refinement levels were programmed and 100 nearly randomly oriented initial grains were used in the simulations with an average grain size of 24 μm, as in the experiment. The 12 $\{1\,1\,1\}\langle 1\,1\,0\rangle$ slip systems were used with rate-sensitive slip with $m = 0.05$.

The modeling frame presented above was applied for simple shear of copper up to a shear of $\gamma = 2$, which is the same strain as in one-pass ECAP in a 90° die. The values of the parameters employed in the simulation work are displayed in Table 1. Some of the parameters were free (indicated in bold letters), so their values were derived from iterative simulation work. The simulation had to reproduce the experimental stress–strain curve (see Fig. 2), the average grain size and the measured average GND density. The crystallographic texture was also reproduced [8].

The stress–strain curves obtained by simulation are displayed in Figure 2a. The strain hardening rate $\theta = d\bar{\sigma}/d\bar{\varepsilon}$ (the so-called Kocks–Mecking plot) was also calculated, and is presented in Figure 2b. The hardening curves were plotted for a set of $C$ parameters (see Eq. (5) for the meaning of $C$) ranging from 0 to 0.5, keeping all the other parameters constant (see Table 1). It is clear

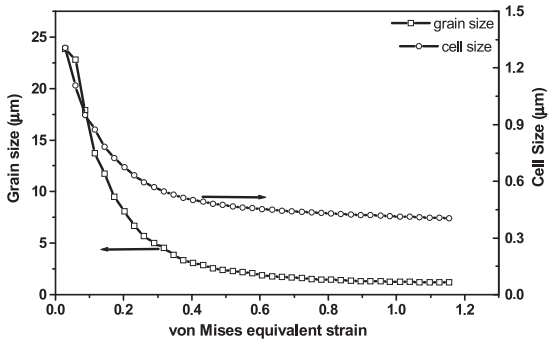


**Figure 3.** Simulated developments of the average grain and cell sizes obtained during one-pass ECAP.

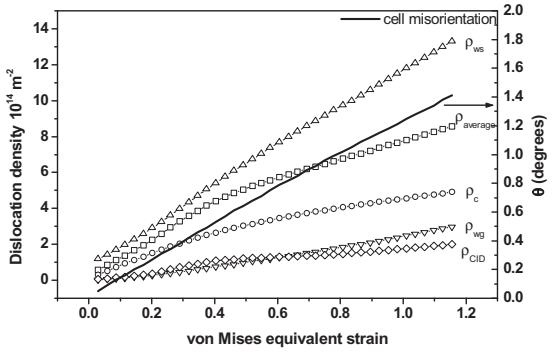


**Figure 4.** The evolution of average dislocation densities in the cell interior ($\rho_c$) and in the cell wall ($\rho_{ws}$ and $\rho_{wg}$), as well as the CID density ($\rho_{\mathrm{CID}}$) as a function of the equivalent strain. The average misorientation angle between adjacent dislocation cells is also plotted.

that the effect of the CID on hardening can be significant if the $C$ parameter is high (Fig. 1). However, the CIDs affect only large strain hardening, starting from an equivalent strain of about 0.35, which is about the beginning of stage IV hardening. The most appropriate value for $C$ is 0.1, where the predicted and experimental strain hardening curves coincide. For $C$ values larger than about 0.3, the flow stress becomes too high with respect to the experiment and the shape of the hardening curve becomes unrealistic. The Kocks–Mecking plots in Figure 2b clearly show that for $C = 0$ there is only stage III, for $C = 0.1$ both stages are well reproduced, while for $C = 0.2$ stage IV begins too early. $C = 0.1$ leads to a predicted CID density of $\rho_{\mathrm{CID}}$ $2.0\times10^{14}\,\mathrm{m}^{-2}$ at the end of straining.

Turning to the predicted grain size and cell size (Fig. 3), the refinement in grain size is significant, decreasing to 1.19 μm from the initial 24 μm. This is in good agreement with the measured value of $1.13 \pm 0.08$ μm. Compared to the changes in grain size, the changes in dislocation cell size are less significant, decreasing from 1.306 to 0.405 μm after one-pass ECAP.

The evolutions of the various predicted dislocation densities are shown in Figure 4. There is a monotonic increase in the dislocation densities as a function of strain and, as expected, it is the cell wall dislocation density that is the highest (its statistical part: $\rho_{ws}$). This variation is remarkable for $\rho_c$, $\rho_{\mathrm{average}}$ and $\rho_{\mathrm{CID}}$. The average value of the dislocation cell misorientation is also plotted in Figure 4 (obtained from $\rho_{wg}$ as defined above) and shows a two-stage aspect reaching a maximum value of 1.41° after one-pass ECAP.

As mentioned above, the CID density is just one component of the GND density: $\rho_{\mathrm{GND}} = \rho_{CID} + \rho_{wg}$. The other component is the dislocation density associated to the cell misorientations ($\rho_{wg}$), which was also predicted by the GR model. Its value at the end of straining was $3.0 \times 10^{14}\,\mathrm{m}^{-2}$ in the simulation. Thus, the predicted total GND density was $5.0\times10^{14}\,\mathrm{m}^{-2}$, which is close to the measured GND value, which was $4.38\times10^{14}\,\mathrm{m}^{-2}$ (Fig. 1). A similar range for the variations of the GND densities was reported in Ref. [20] for Al.

In conclusion, it is demonstrated in the present paper that GNDs significantly affect stage IV, in agreement with the findings of Pantleon [6,7], who used a different approach. What is new in our approach is that the GND density comes directly from a polycrystal plasticity grain refinement model and that this density compares well to experimental findings. It is also shown experimentally in this work that the CID dislocations periodically group into walls.

The authors are grateful to Dr. Wolfgang Pantleon (Riso National Laboratory, Denmark) for his valuable comments. C.F.G. acknowledges the Université Paul Verlaine de Metz, France (2011) for a visiting position. B.B. is grateful to the Alexander von Humboldt Foundation for his research fellowship.

[1] U.F. Kocks, In: Dislocations and Properties of Real Materials, Institute of Metals, Proceedings of the Conference to Celebrate the Fiftieth Anniversary of the Concept of Dislocation in Crystals. London, 1985, pp. 125–143.
[2] U.F. Kocks, J. Eng. Mater. Technol. 98 (1976) 76–85.
[3] Y. Estrin, L.S. Tóth, A. Molinari, Y. Bréchet, Acta Mater. 46 (1998) 5509–5522.
[4] L.S. Tóth, A. Molinari, Y. Estrin, J. Eng. Mater. Technol. 124 (2002) 71–77.
[5] A.D. Rollett, Strain Hardening at Large Strains in Aluminum Alloys, Ph.D. thesis, Department of Materials Engineering, Drexel University, Philadelphia, PA, 1988.
[6] W. Pantleon, Mater. Sci. Eng. A 387–389 (2004) 257–261.
[7] W. Pantleon, Mater. Sci. Eng. A 400–401 (2005) 118–124.
[8] L.S. Tóth, Y. Estrin, R. Lapovok, C. Gu, Acta Mater. 58 (2010) 1782–1794.
[9] C.F. Gu, L.S. Tóth, B. Beausir, T. Williams, C.H.J. Davies, Mater. Sci. Forum 654–656 (2010) 1570–1573.
[10] C.F. Gu, L.S. Tóth, R. Lapovok, C.H.J. Davies, Philos. Mag. 91 (2011) 273–290.
[11] C.F. Gu, L.S. Tóth, M. Arzaghi, C.H.J. Davies, Scripta Mater. 64 (2011) 284–287.
[12] C.F. Gu, L.S. Tóth, C.H.J. Davies, Scripta Mater. 65 (2011) 167–170.
[13] Y. Estrin, L.S. Tóth, Y. Bréchet, H.S. Kim, Mater. Sci. Forum 503–504 (2006) 675–680.
[14] A. Nadai, Theory of Flow and Fracture of Solids, 2nd edn, McGraw- Hill, New York, 1950.
[15] J.F. Nye, Acta Metall. 1 (1953) 153–162.
[16] W. Pantleon, Scripta Mater. 58 (2008) 994–997.
[17] B. Beausir, J.J. Fundenberger, Software for Orientation Image Mapping, <http://benoitbeausir.free.fr>.
[18] D.A. Hughes, Q. Liu, D.C. Chrzan, N. Hansen, Acta Mater. 45 (1997) 105–112.
[19] D.L. Holt, J. Appl. Phys. 41 (1970) 3197–3201.
[20] B.S. El-Dasher, B.L. Adams, A.D. Rollett, Scripta Mater. 48 (2003) 141–145.